Non-Contact Blood Pressure Monitoring using Dual mm-Wave Radar Sensors with Machine Learning

Srikrishna Ramesh Iyer[1], Leo Zhao[2], Manoj Prabhakar Mohan[3], Mohammad Yakoob Siyal[1,3], Arokiaswami Alphones[1,3], Liu Ai Qun[1], and Muhammad Faeyz Karim[1,3*]

[1]School of Electrical and Electronic Engineering, Nanyang Technological University (NTU), 50 Nanyang Avenue, Singapore 639798.

[2] NCS Corporation, Singapore.

[3]Singtel Cognitive and Artificial Intelligence Lab for Enterprises (SCALE@NTU), Nanyang Technological University (NTU), Singapore.

[*]faeyz@ntu.edu.sg

Abstract

A novel dual-mmWave radar sensor for non-contact blood pressure (BP) monitoring is presented in this work. The proposed system utilizes two mmWave radars, one that is pointed towards the chest while the other is oriented towards the neck. The heart rate frequencies from the chest and carotid arteries (neck) are extracted from the phase signals reflected from the human body. The Systolic (SBP) and diastolic blood pressure (DBP) is estimated using an optimized machine learning regression model trained using statistical features based on pulse transit time (PTT). A Gaussian SVM model was trained using an open-source ECG-PPG dataset comprising 26 test subjects who's age range between 21 to 50 years. The trained model metrics are presented and further optimized using random search technique to obtain R^2 values of 0.91 and 0.97 for SBP and DBP respectively. The trained model was then used to test PTT-based features extracted from radar phase signals for predicting SBP and DBP values. To determine the ideal range of measurement, the model was tested at distances ranging between 30 cm-150 cm and results were analyzed in comparison to a cuff-based reference device using evaluation parameters that include standard deviation, P-statistic, correlation coefficient (R), root mean square (RMSE) value, mean absolute error (MAE) and median absolute error (MedAE). It was found that for 30 cm-120 cm, the R values lie in the range, (0.632,0.839) for SBP and (0.653,0.908) for DBP in comparison to the ground truth. The standard deviation and MAE values were also found to be well within the maximum limit in accordance with AAMI/ESH/ISO standards. It was observed that the ideal range of a contactless BP detection system is 30 cm-90 cm away from a body.

Introduction

Cardiovascular diseases are the leading cause of deaths in Singapore for the past three years accounting to over 30% of the deaths[1]. Worldwide, the number of people affected by blood pressure-based disorders like hypertension and hypotension is expected to rise to over 1.5 billion by 2025[2]. Detection and prevention of cardiovascular diseases involves measurement of vital signs that include, temperature, blood pressure, breathing rate, pulse rate and dissolved O_2. However, wearables in most health care institutions continue to use invasive or contact-based systems for single-point blood pressure monitoring. Home-based standard

measurement systems consist of contact-based sphygmomanometers which use cuffs[3]. More accurate systems used in hospitals involve invasive (intra-arterial) insertion of cannula needles in the artery[4]. Hence, a non-contact, non-invasive system of BP measurement is required to facilitate a comfortable system of monitoring for patients without having to worry about inconvenient contact sensors and elaborate device connections. Several non-invasive methods have been introduced based on pulse transit time (PTT), pulse arrival time (PAT) and pulse wave velocity (PWV) which utilize a combination of two devices/sensors some of which include two PPG's (photoplethysmography)[5], BCG (Ballistocardiograph) and PPG[6], mobile phone sensors[7], magneto-plethysmograph sensors[8], skin-based microelectromechanical sensors[9], wearable watches like OMRON heartguide, Asus vivowatch[10], wearable glasses[11] and bioimpedance sensors[12]. PTT is an increasingly popular metric used for blood pressure prediction. As illustrated in Figure 1, It is the time it takes for a pulse pressure signal to flow between a proximal and a distal point on an arterial network. If the distance between the two points is known, then the PWV is obtained. PAT is equal to the sum of PTT and pre-ejection period (PEP).

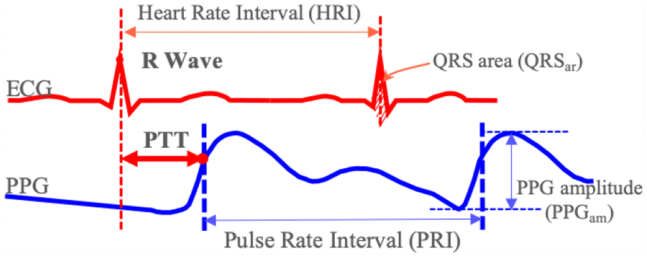

Figure 1. PTT using ECG and PPG signals

Wibmer T et al. show that PAT can be measured as the time interval between the R-peak of an ECG and corresponding upstroke of a PPG from the tip of a finger[13]. Another work involved usage of signals from dual PPG sensors placed on the wrist and shoulder to estimate PTT[14]. Several studies have shown that there exists a relationship between PTT and PWV with Systolic diastolic pressure (SBP) and diastolic blood pressure (DBP). Wibmer T et al. studied results based on 20 subjects and established the relationship between SBP and PTT using regression techniques[13]. Linear relationship between PAT and blood pressure is established on 96 hours of testing 11 ICU patients[15]. It was concluded that this relation holds good only for long durations of measurement and high BP values. Furthermore, according to a study[16], PAT-based BP produced poor results that did not meet the FDA BP error limits. Several mathematical models have already been established between PTT and BP[17-20]. According to the Moens-korteweg equation[19-20], BP and PTT are physiologically related. When PTT decreases, the arterial elastic modulus increases which in turn increases the blood pressure. This allows us to monitor BP through a well-known PTT based approach for Hypertension detection and diagnosis[22].

Current contact-based sensor systems are too uncomfortable and inconvenient to use especially for continuous ambulatory BP monitoring. Contact sensors like the ECG, PPG, BCG etc. are inaccurate due to additive noises arising from random bodily movements and their vulnerability to water, dust, sweat or external contaminants that may render the sensors faulty[23]. Hence, there arises a need to present a non-contact, non-invasive system that eliminates usage of uncomfortable insertion of catheters or usage of contact-based sensors and wearable device connections. Recently, several radar-based systems have been proposed for non-contact measurement of heart rate and respiration rate. Consequently, the types of radars used for this application include continuous-wave (CW) doppler radars[24-34], Impulse radio Ultra-wideband (IR UWB) radars[35-36] and frequency modulated continuous wave (FMCW) doppler radars[37-40]. All current systems for vital signs monitoring using radars are predominantly used to detect heartbeat and breathing rates. Moreover, some BP monitoring systems use radars in combination with a contact-based sensor utilize

BP markers like PTT, PAT or PWV as described earlier. An on-body CWR (Continuous wave radar) in tandem with a PPG sensor was used to estimate blood pressure using PAT[41-42]. Another system utilized a combination of CW radars and bio impendence contact sensors to measure BP using PTT[43]. A single radar-based system was proposed[44] which formulated a linear mathematical relationship between DBP, and fall-time of a phase signal obtained from the radar. This relation is formed based on contraction and expansion of the heart, PWV and diameter change in arteries due to blood flow. The estimated BP was compared to a cuff-based monitor and their results were validated solely based on correlation coefficient. However, the evaluation metrics were not in accordance with the standards for non-invasive BP measurement put forth by AAMI/ESH/ISO[45]. To the best of our knowledge, a reliable system of monitoring BP using radars is yet to be proposed.

This paper aims to propose a novel non-contact dual radar-based BP measurement system that utilizes PTT to measure SBP and DBP. This involves detecting phase variations at two points on the body namely, distal (carotid artery at the neck) and proximal (chest) points. The time interval between the arrival of peak phase values is computed as PTT which is then used to predict SBP and DBP values using Gaussian SVM regression algorithm. The predicted BP values were measured at varying distances (30cm-150cm) to determine the optimal range of measurement. Results were validated with a cuff-based BP monitoring device and comparisons were made based on standard deviation, P-statistic, correlation coefficient (R), root mean square (RMSE) value, mean absolute error (MAE) and median absolute error (MedAE).

Proposed Method of measuring blood pressure

System description

This paper introduces a novel system of monitoring blood pressure using dual mm-wave radars based on Pulse transit time (PTT) as shown in Figure 2. Phase signals are extracted from two mm-wave radars A & B pointed toward the chest and neck. The radar B pointed towards the neck region measures the tiny displacements of the carotid artery due to blood flow while radar A pointed towards the chest, measures the displacements due to heartbeat and breathing.

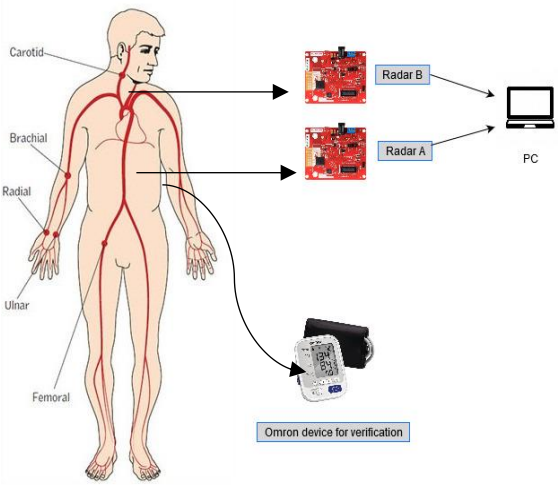

Figure 2. Proposed setup of blood pressure measurement

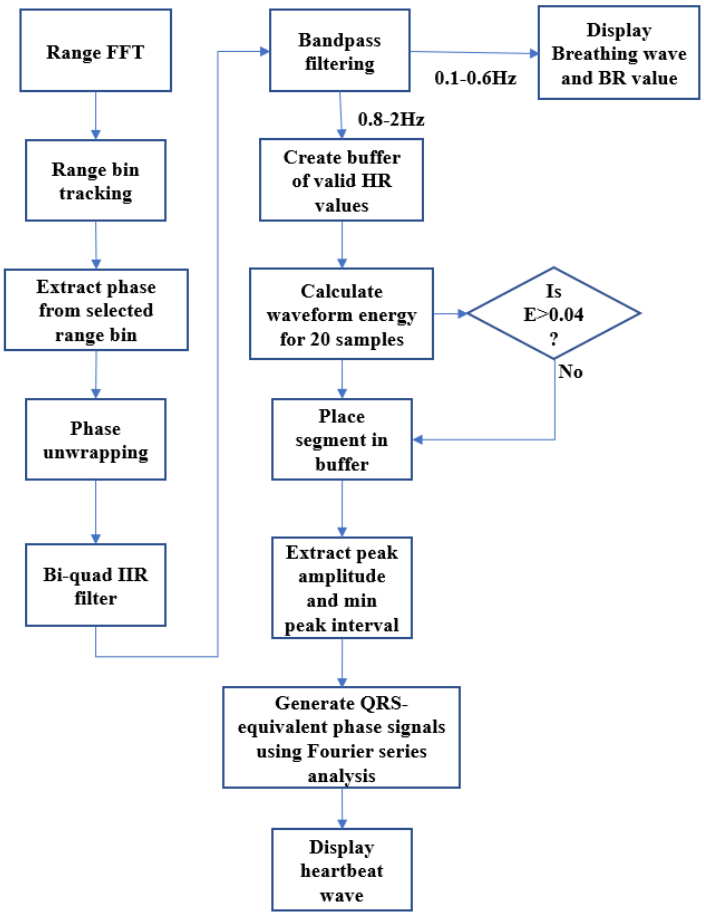

Figure 3. Signal processing flow

Each chirp signal sampled at the beat frequency f_b is converted to a complex range profile by applying the range FFT[17]. Range profiles of multiple chirp signals are stacked on top of each other and converted into a matrix with i number of rows (fast time samples) and j columns (slow time samples). Since, vital signs are detected for a stationary person, the phase change across the slow time axis is extracted from a single range bin. Phase unwrapping algorithm is then implemented to restrict the phase difference values to fall in $[-\pi, \pi]$. After filtering impulse noise due to phase unwrapping, the phase values are passed through a serially cascaded Bi-Quad IIR filter. Finally, the breathing and heartbeat waves are obtained as shown in Figure 3. Additionally, for our experiment, we propose a QRS signal generation module which extracts the signal peaks and base time of the heartbeat phase signal to generate QRS-like signals using Fourier series representation of triangular waveforms. Thus, eliminating signal overshoots, aperiodicity and improving the SNR value of the extracted signal. Signal pre-processing[56] is utilized to filter the breathing wave signal from the heartbeat signal.

As described in Figure 4, after the required neck pulse waveforms and heartbeat signals are extracted, peak detection is performed to extract PTT-based features. PTT is obtained by estimating the time between two consecutively occurring peaks observed in the neck pulse and heartbeat waveforms. Since there are no readily available radar-based phase signals of vital signs, an open-source ECG-PPG signal dataset is used to train a machine learning model to predict SBP and DBP values. Standard signal processing steps were employed to remove artefacts in the raw ECG and PPG signals.

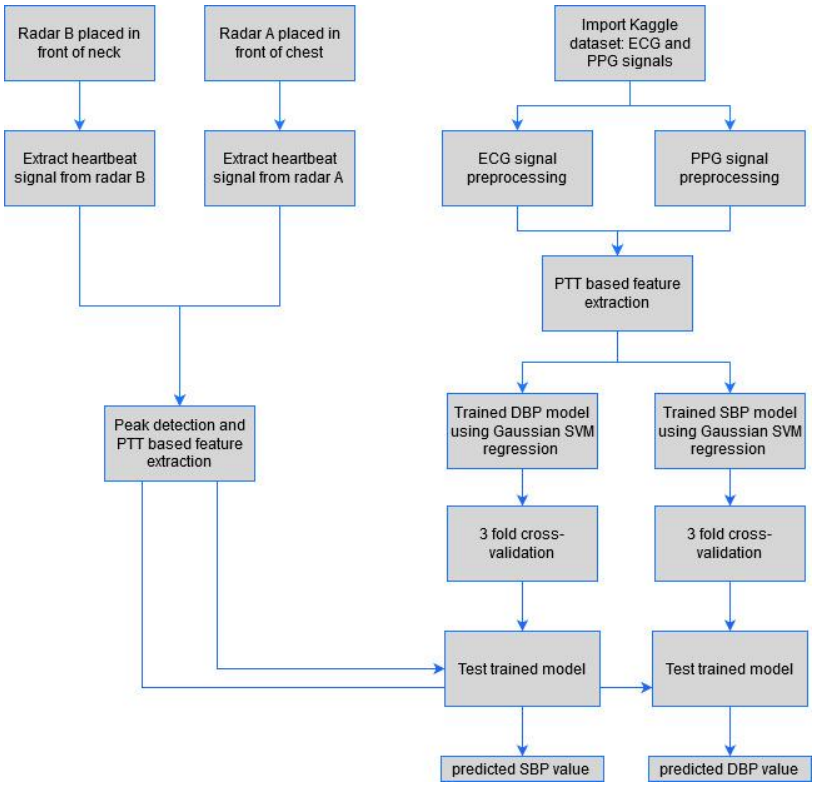

Figure 4. Work flow for the detection of blood pressure

Most ECG signal components lie in the 5~100Hz frequency range[46]. Hence, pre-processing allows us to filter out several artefacts commonly found in ECG signals. Muscle tremor artifacts caused due to shivering or sudden body movements (usually in the elderly) are high frequency signals 30~300Hz that is removed by low pass filters[48]. The 50~60Hz electromagnetic interference (EMI) is removed by a band-stop filter[47]. Lastly, baseline wander is an ultra-low frequency signal that ranges between 0~0.5Hz that can be eliminated using a high-pass filter[49]. The signal specifications and their corresponding method of removal is summarized in Table I.

Table I: Signal specifications of ECG signal

	Artefact	Frequency	Method of removal
1	Muscle tremor	30~300Hz	Butterworth Low pass
2	EMI	50~60Hz	Notch filter
3	Baseline wander	0~0.5Hz	4^{th} order Butterworth high pass[49]

Since the signals were extracted from a wearable finger clip-based PPG sensor, removal of signal distortion due to motion artifact is a major challenge to overcome. Frequency of a PPG signal normally lies in the range 0.5-5Hz while for motion artifacts it lies in 0.01-10Hz[50]. There are several adaptive noise reduction techniques which include moving average filter, median filter, adaptive noise cancellation[51], wavelet transform[52], Independent component analysis[53], singular value decomposition[54] and cycle Fourier series analysis[55]. In this paper, the moving median filter is used to remove motion artifact since it has the least computation time.

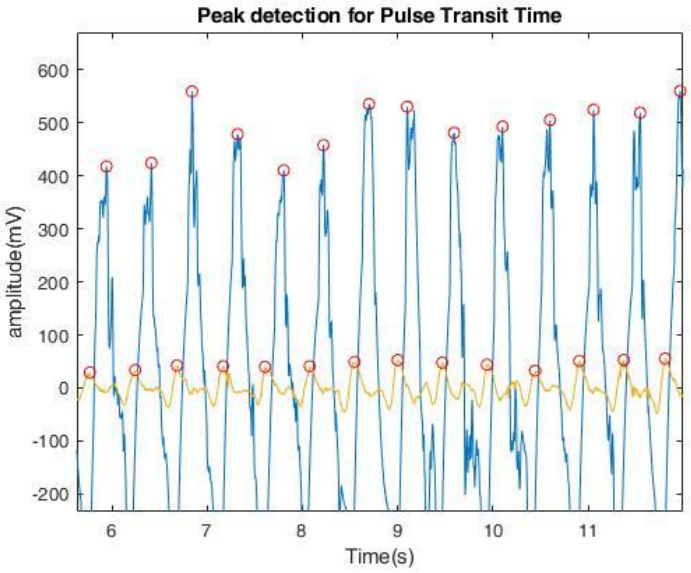

Figure 5. PTT extraction from ECG (blue) and PPG (yellow)

Experimental setup

In this work Texas Instrument (TI's) IWR1443BOOST FMCW radar-based evaluation module (EVM) that operates in the 76-81 GHz band is used. The system uses a combination of 2 IWR boards of 5V DC supply, each consisting of 4 receiving antennas (Rx) and 3 transmitting antennas (Tx) contained in the RF/analog subsystem. The subsystem also consists of an ADC buffer which stores the ADC outputs of received IF signals. These outputs are then processed by extracting the change in phase in a range bin from the 1D FFT (fast-time axis). The hardware setup consists of two radars connected to a PC directed towards the neck (carotid artery) and chest at a human test subject as shown Figure 6.

Figure 6. Measurement setup for BP estimation

Dataset

A non-invasive blood pressure dataset from kaggle[56] was used to train a regression model. The dataset consists of PPG, ECG, force sensing resistor (FSR), and Phonocardiogram (PCG) signals with the corresponding SBP and DBP values. The dataset was formed using 26 test subjects in the age range, 21-50 years. In this work, the feature extraction, signal processing and machine learning was implemented using MATLAB R2020. As outlined in Figure 5, after filtering out low and high frequency artifacts, R peaks in the ECG signal and peaks in PPG signal are detected and the PTT is measured as,

$$\text{Average PTT}\mu_{PTT} = \frac{\sum_{i=1}^{n} PTT_i}{n} \tag{1}$$

$$\text{Normalized max difference} = \frac{\max(PTT) - \min(PTT)}{\mu_{PTT}} \tag{2}$$

$$\text{Root mean square of successive differences, RMSSD} = \sqrt{\frac{\sum_{i-2}^{n}(PTT_i - PTT_{i-1})^2}{n-2}} \tag{3}$$

$$\text{Coefficient of variation} = \frac{\sigma_{PTT}}{\mu_{PTT}} \tag{4}$$

$$\text{Normalized absolute deviation} = \frac{\sum_{i=1}^{n} \frac{|PTT_i - \mu_{PTT}|}{PTT}}{n} \tag{5}$$

In addition to the above features, age and BMI is included as training features. A SBP and a DBP database created using PTT based features extracted from the PPG and ECG signals. The DBP and SBP databases have the same training features but are trained separately since it is a single output regression problem. The relationship between predicted SBP and DBP values still hold good as the training features used are the same.

Training regression model

The diastolic blood pressure (DBP) database was trained with 14 regression algorithms and compared based on minimization of root mean square error (RMSE), regression coefficient (R^2), mean square error (MSE), mean absolute error (MAE) and training time, in seconds. The algorithms were cross validated using 3-fold cross-validation. The evaluation metrics for training algorithms on the SBP and DBP datasets are shown in Table II and Table IV respectively. Hence, the model trained by Gaussian SVM regression algorithm was used as our regression model for SBP and DBP prediction. From Table II and Table IV, Gaussian SVM clearly outperforms other algorithms based on minimization of RMSE & MAE and maximization of the regression coefficient. Gaussian SVM uses a non-linear kernel function (gaussian function) to classify our non-linearly separable data.

Hyperparameter tuning is performed to optimize the selected regression model (Gaussian SVM). The tunable parameters which include Kernel scale, box constraint and epsilon value are tuned for 30 iterations using random search optimization. The minimum MSE plot in Figure 7 shows the gradually decreasing MSE for every iteration number. Unlike Bayesian optimization, where a set of hyperparameters are chosen such that it minimizes an upper confidence level of the objective function i.e. MSE., we obtain a single set of hyperparameters using random search optimization, It is observed that the best point hyperparameters and minimum error hyperparameters are the same where the MSE value is reduced to 16.16 as shown in Figure 7.

Table II: Evaluation metrics of training algorithms for SBP

Regression model	RMSE	R^2	MAE	Training time (s)
Linear regression	11.523	0.27	8.82	0.18
Linear regression (Interactions linear)	7.35	0.7	4.8	0.08
Linear regression (Robust linear)	11.7	0.25	8.55	0.07
Stepwise linear regression	12.11	0.2	9.21	1.11
Regression fine tree	8.39	0.61	6.76	**0.052**
Regression medium tree	12.049	0.21	8.87	**0.052**
Linear SVM	12.082	0.2	8.74	0.057
Quadratic SVM	8.87	0.57	6.2	0.053

Cubic SVM	7.58	0.69	4.58	0.08
Gaussian SVM	**6.12**	**0.8**	**3.3**	0.058
Medium Gaussian SVM	9.351	0.52	6.44	0.054
Boosted trees	11.17	0.32	8.42	0.22
Bagged Trees	11.562	0.27	9.45	0.23
Exponential gaussian process regression	13.52	0	11.165	0.08

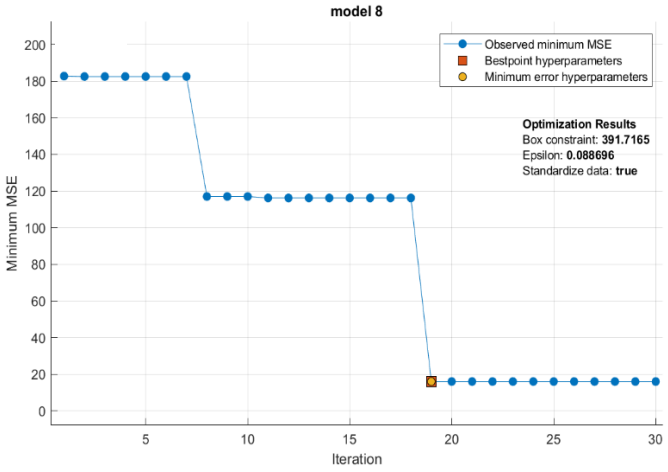

Figure 7. Hyperparameter tuning of Gaussian SVM model for SBP using random search optimization

The evaluation results are compared based on three optimization techniques as outlined in Table III. Since Baeysian optimization yields a trained model with RMSE ≈ 0 and R^2=1, it can be inferred that the model is overfit and cannot be utilized to predict SBP values that deviate from the mean observations i.e. <120 and >130. Hence, Random search is selected over other techniques for hyperparameter tuning.

Table III: Hyperparameter tuning of Gaussian SVM for SBP

Optimization Technique	**Random search**	Bayesian	Grid search
RMSE	**4.02**	0.67	5.01
R^2	**0.91**	1	0.86
MAE	**1.405**	0.45	1.85

Training time (s)		**15.157**	112.68	51.617
Optimization results	Box constraint	**391.72**	994.92	1000
	Epsilon	**0.088**	0.68	0.67

In Table IV, regression algorithms are evaluated for prediction of DBP values. As mentioned earlier, Gaussian SVM outperforms other algorithms with the highest R^2 value of 0.95 and the least RMSE value of 2.058.

As implemented before, Gaussian SVM is optimized using Random search, Bayesian and Grid search techniques to minimize the objective function i.e. mean square error. From Table V, the same hyperparameters are tuned and evluation results are presented. However, after 30 iterations, both Bayesian and Grid search optimization fail to converge to the local minima while random search produced better results with reduced RMSE value from 2.058 to 1.495 and an improvement in the R^2 value from 0.95 to 0.97

Table IV: Evaluation metrics of training algorithms for DBP

Regression model	RMSE	R^2	MAE	Training time (s)
Linear regression	6.89	0.4	5.79	1.704
Linear regression (Interactions linear)	4.47	0.75	3.617	0.292
Linear regression (Robust linear)	6.89	0.4	5.78	0.29
Stepwise linear regression	6.33	0.5	5.18	1.514
Regression fine tree	5.13	0.67	4.24	0.437
Regression medium tree	8.216	0.15	6.29	0.08
Linear SVM	7.51	0.29	5.94	0.147
Quadratic SVM	5.76	0.58	4.183	0.058
Cubic SVM	4.129	0.79	2.64	0.059
Gaussian SVM	**2.058**	**0.95**	**1.55**	0.117
Medium Gaussian SVM	5.11	0.67	3.65	0.07

Boosted trees	5.9	0.56	5.025	0.867
Bagged Trees	6.539	0.46	5.5	**0.509**

As outlined in Table V, random search is implemented for hyperparameter tuning and the gradual minimization of MSE for trained DBP model is plotted in Fig. 8. As before, the bestpoint and minimum error hyperparameters are the same where the MSE value is reduced to 2.23 which is clearly an improvement from the MSE value of 4.23 before optimization

Effect of distance on BP measurement

The SBP and DBP values are estimated by the dual-radar system at varying testing conditions in comparison to a reference OMRON device to determine ideal measurement setup requirements. The Radar system is tested at varying distances and BP values are recorded at d = 30 cm, 60 cm, 90 cm, 120 cm & 150 cm as shown in Table VI to determine the ideal range for accurate BP measurement. For every distance measured i.e. d=30 cm, 60 cm, 90 cm, 120 cm & 150 cm, 10 observations were recorded for a single test subject. Each BP value is color coded based on their diagnosis results. Green denotes normal blood pressure, yellow denotes elevated BP and Red indicates hypertension stage-I. Each radar observation lasted for 25.6s while that of OMRON takes approximately 60s to obtain the BP outputs. For every observation recorded by the radar system, a corresponding SBP & DBP value is recorded by OMRON. Each set of observations are interleaved with 1 min of resting time. Table VII-XI outline the evaluation metrics to determine the ideal distance for BP measurement.

Table V: Hyperparameter tuning of Gaussian SVM for DBP

Optimization algorithm		**Random search**	Bayesian	Grid search
RMSE		**1.495**	3.43	3.48
R^2		**0.97**	0.85	0.85
MAE		**0.472**	1.26	1.29
Training time (s)		**42.056**	78.081	16.23
Optimization results	Box constraint	**68.68**	999.14	1000
	Epsilon	**0.035**	0.039	0.036

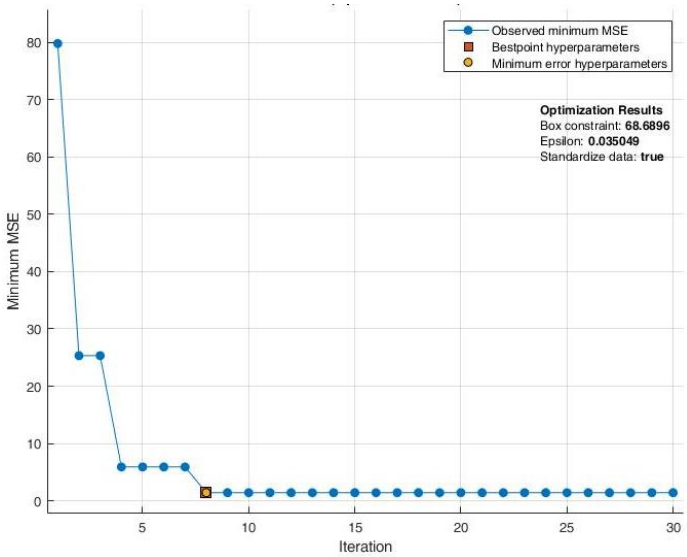

Fig. 8: Hyperparameter tuning of Gaussian SVM model for DBP using random search optimization

Table VI: BP for different ranges of measurement

distance (cm)	Device	BP	Observations 1	2	3	4	5	6	7	8	9	10	Diagnosis (majority)
30	Radar	SBP	117	120	121	120	126	118	121	120	117	120	Normal BP
		DBP	76	80	83	79	78	73	80	79	80	80	
	OMRON	SBP	116	116	120	119	122	111	119	118	113	116	Normal BP
		DBP	78	83	84	73	78	75	80	78	80	78	
60	Radar	SBP	121	123	122	120	124	121	121	121	122	128	Elevated BP
		DBP	77	75	78	74	76	79	76	80	79	77	
	OMRON	SBP	121	123	120	120	120	122	120	123	121	125	Elevated BP
		DBP	76	77	79	76	79	80	76	80	81	80	
90	Radar	SBP	123	122	132	123	118	124	124	124	123	123	Elevated BP
		DBP	75	81	78	79	75	76	71	70	71	70	
	OMRON	SBP	125	122	130	124	122	123	123	120	120	122	Elevated BP
		DBP	77	79	80	82	75	74	72	72	72	71	
120	Radar	SBP	124	119	123	116	120	121	118	128	120	126	Uncertain
		DBP	73	75	80	70	80	83	80	78	73	79	
	OMRON	SBP	122	116	120	119	118	118	117	126	116	122	Normal BP
		DBP	78	77	79	76	80	81	77	80	75	81	
150	Radar	SBP	123	124	134	132	130	131	112	111	112	123	Uncertain
		DBP	70	73	82	83	86	70	72	69	72	74	
	OMRON	SBP	116	115	115	119	117	113	120	121	120	118	Normal BP
		DBP	78	75	76	74	76	74	77	83	81	75	

The evaluation metrics include, standard deviation, p statistic, correlation coefficient, RMSE value, MAE and MedAE. In an ideal scenario, both the radar and OMRON BP values must be equal i.e. the regression coefficient R^2 should be 1. However, in most cases, this might not be possible hence, according to AAMI/ESH/ISO[45] standards for non-invasive BP measurement, the MAE and standard deviation values should be <5mmHg and <8mmHg respectively. Our experimental results show that distances 30 cm, 60

cm, 90 cm and 120 cm are well within the AAMI standards for non-invasive BP measurement. Thus, we can conclude that ranges 30-120cm are suitable for BP measurement using our dual radar system. To further support this claim, the p-values and R can be analysed for 10 observations. Consider a null hypothesis which states that there is simply no relation between the radar-based and OMRON-based SBP & DBP values. If the p value obtained is <0.05, then we can safely conclude that the probability of accepting the null hypothesis is low i.e. we can safely reject the null hypothesis. For example, in Table VII, the p-value for SBP is 0.004 which implies that there is a probability of 0.004 of accepting the null hypothesis. Since this probability is too low, we can safely reject the null hypothesis thereby inferring that there exists a linear relationship between the radar-based and OMRON-based SBP values. Thus, we can similarly reject the null hypothesis for range values = 30 cm, 60 cm, 90 cm,120 cm, who's p-values are clearly less than 0.05. The coefficient of variation signifies how strongly the dependent (radar-based BP) and independent (OMRON-based BP) variables are related. The maximum R value for SBP and DBP measurement is obtained when the Range is 30 cm and 90 cm respectively. As expected, for 30 cm-120 cm, a positive correlation coefficient is obtained but a negative R value of -0.73 and -0.44 is found at 150 cm. This proves that there exists a negative correlation between the BP values estimated by radar and OMRON at 150 cm thereby justifying the rejection of the null hypothesis previously considered.

Table VII: Evaluation metrics, Range = 30 cm

Range=30cm					
SBP			DBP		
Metric	OMRON	Radar	Metric	OMRON	Radar
Avg SBP	117	120	Avg DBP	78.7	78.8
Std	3.29983	2.581	Std	3.30151	2.6997
p-value		0.004	p-value		0.0406
R		0.808	R		0.653
RMSE		3.521	RMSE		2.42
MAE		3	MAE		1.7
MedAE		3	MedAE		1.5

Table VIII: Evaluation metrics, Range = 60 cm

Range=60cm					
SBP			DBP		
Metric	OMRON	Radar	Metric	OMRON	Radar
Avg SBP	121.5	122.3	Avg DBP	78.4	77.1
Std	1.7159	2.311	Std	1.9550	1.911
p-value		0.05	p-value		0.0106
R		0.632	R		0.761
RMSE		1.89	RMSE		1.81
MAE		1.4	MAE		1.5
MedAE		1	MedAE		1.5

Table IX: Evaluation metrics, Range = 90 cm

Range=90cm					
SBP			DBP		
Metric	OMRON	Radar	Metric	OMRON	Radar
Avg SBP	123.1	123.6	Avg DBP	75.4	74.6
Std	2.8848	3.438	Std	3.893	3.977
p-value		0.016	p-value		0.0284
R		0.732	R		0.908
RMSE		2.3	RMSE		1.78
MAE		1.9	MAE		1.6
MedAE		1.5	MedAE		2

Table X: Evaluation metrics, Range = 120 cm

Range=120cm					
SBP			DBP		
Metric	OMRON	Radar	Metric	OMRON	Radar
Avg SBP	119.4	121.5	Avg DBP	78.4	77.1
Std	3.169	3.719	Std	2.118	4.121
p-value		0.002	p-value		0.011
R		0.839	R		0.758
RMSE		2.84	RMSE		3.016
MAE		2.7	MAE		2.5
MedAE		3	MedAE		2

Table XI: Evaluation metrics, Range = 150 cm

Range=150cm					
SBP			DBP		
Metric	OMRON	Radar	Metric	OMRON	Radar
Avg SBP	117.4	123.2	Avg DBP	76.9	75.1
Std	2.633	8.829	Std	2.998	6.172
p-value		0.0165	p-value		0.199
R		-0.73	R		-0.44
RMSE		11.85	RMSE		7.77
MAE		11	MAE		6.8
MedAE		9.5	MedAE		7

From Table VI, both range = 120 cm and range =150 cm produce uncertain diagnostic results. For 150 cm, both Hypertension stage-I and normal BP are tied at 4 observations each. Based on this deviation in the diagnostic results, we can conclude that 150 cm is unsuitable for measurement of our 77 GHz radar system. Additionally, we also observe uncertainty in diagnosis for 120 cm as 5 out of 10 observations recorded by the radar are normal while the remaining 5 observations show that they are elevated BP values. This clearly contradicts our evaluation results as shown in Table X where we obtained high R values of 0.839 and 0.758 for SBP and DBP respectively. This is because, the RMSE between radar and OMRON values is high i.e. the deviation between them is very high at 2.84 for SBP and 3.016 for DBP. Hence, if the radar values are closer to its mean, there may be a possibility that the high R value is misleading as the SBP and DBP values predicted are uniform about its mean with a large deviation from the ground truth. Hence, it can be concluded that the 30 cm-90 cm range is ideal for BP measurement using the proposed system. However, it was found that there were some contradictions at 120 cm when the final diagnostic result was uncertain even though the R value was quite high, and p was lesser that 0.05. Possible solutions may involve taking more observations (currently number of training examples are only 26) from different test subjects of all age groups and genders. This will increase the size of the dataset and help train a more robust regression model thereby reducing uncertainties while diagnosis.

Conclusion

A dual radar-based contactless system is proposed for continuous monitoring of blood pressure (systolic and diastolic blood pressure) using mm-wave wave radars operating in the 77 GHz frequency range. The proposed system is implemented using an indicator PTT which is extracted from an open-source ECG-PPG dataset. The extracted features were used to train and compare several regression models out of which Gaussian SVM regression was selected and its hyperparameters were tuned using random search method. Finally, the trained model was tested for varying distances to determine the ideal distance of measurement between the person and the radar system. It was found that 30 cm-90 cm was the ideal range of measurement for BP based on evaluation parameters that included standard deviation, p statistic, correlation coefficient, RMSE value, MAE and MedAE. For 30 cm-90 cm, the p-value was less than 0.05 and the MAE & standard deviation was much lower than the AAMI standards.

Ethical approval

All procedures performed in studies involving human participants were in accordance with the ethical standards of Singtel Cognitive and Artificial Intelligence Lab for Enterprises (SCALE@NTU) and with the 1964 Helsinki declaration and its later amendments or comparable ethical standards.

Informed consent

Informed consent was obtained from all individual participants included in the study.

References

1. https://www.moh.gov.sg/resources-statistics/singapore-health-facts/principal-causes-of-death
2. Perkovic, V., Huxley, R., Wu, Y., Prabhakaran, D., & MacMahon, S. The burden of blood pressure-related disease: a neglected priority for global health. *Hypertens.*, **50**, 991–997, (2007).

3. IEEE standard for wearable cuffless blood pressure measuring devices. *IEEE Std 1708-2014*, 1–38, (2014).
4. White, L., Halpin, A., Turner, M., & Wallace, L. Ultrasound-guided radial artery cannulation in adult and paediatric populations: a systematic review and meta-analysis. *British journal of anaesthesia*, **116**, 610–617, (2016).
5. Wong, M. Y., Poon, C. C., & Zhang, Y. T. An evaluation of the cuffless blood pressure estimation based on pulse transit time technique: a half year study on normotensive subjects. *Cardiovascular engineering (Dordrecht, Netherlands)*, **9**, 32–38, (2009).
6. Martin, SO., Carek, A., Kim, CS. et al. Weighing Scale-Based Pulse Transit Time is a Superior Marker of Blood Pressure than Conventional Pulse Arrival Time. *Sci Rep* **6**, 39273, (2016).
7. Anchan, R. Estimating pulse wave velocity using mobile phone sensors. Bachelor's thesis, Edith Cowan University (2011).
8. Lee, Y.-J. et al. Magneto-plethysmographic sensor for peripheral blood flow velocity. *IEEE Sensors j*. **14**, 1341–1342 (2014).
9. Hsu, Y.-P. & Young, D. J. Skin-coupled personal wearable ambulatory pulse wave velocity monitoring system using microelectromechanical sensors. *IEEE Sensors J*. **14**, 3490–3497 (2014).
10. Thomas, S. S. et al. Biowatch: A noninvasive wrist-based blood pressure monitor that incorporates training techniques for posture and subject variability. *IEEE j. Biomed Heal. Informatics* **20**, 1291–1300 (2016).
11. Holz, C and Wang, E. J.. Glabella: Continuously Sensing Blood Pressure Behavior using an Unobtrusive Wearable Device. *Proc. ACM Interact. Mob. Wearable Ubiquitous Technol.* **1**, 3, Article 58, 1- 23. (2017)
12. Heydari, F. et al. Continuous cuffless blood pressure measurement using body sensors. *13th International Conference of Body Area Network (BodyNets) of EAI*, Finland, Oulu (2018).
13. Wibmer, T. et al. Pulse transit time and blood pressure during cardiopulmonary exercise tests. *Physiol. Res.*, **63**(3), 287–296, (2014).
14. Wang, Y., Liu, Z., & Ma, S. Cuff-less blood pressure measurement from dual-channel photoplethysmographic signals via peripheral pulse transit time with singular spectrum analysis. *Physiol. Meas.*, **39**(2), 025010, (2018).
15. Escobar-Restrepo, B., Torres-Villa, R., & Kyriacou, P. A. Evaluation of the Linear Relationship Between Pulse Arrival Time and Blood Pressure in ICU Patients: Potential and Limitations. *Front. Physiol.*, **9**, 1848, (2018).
16. Zhang, G., Gao, M., Xu, D., Olivier, N. B., & Mukkamala, R. Pulse arrival time is not an adequate surrogate for pulse transit time as a marker of blood pressure. *J. Appl. Physiol.*, **111**, 1681–1686, (2011).
17. Bazett, H. C. & Dreyer, N. B. Measurements of pulse wave velocity. *American Journal of Physiology-Legacy Content* **63**(1), 94-116, (1922).
18. Bramwell, J. C., Downing, A. C., & Hill, A. V. The effect of blood pressure on the extensibility of the human artery. *Heart*, **10**(4), 289-300, (1923).
19. Noordergraaf, A. The arterial tree: in Circulatory System Dynamics. New York: Academic press 137-139, (1978).
20. Pruett, J. D., Bourland, J. D., & Geddes, L. A. Measurement of pulse-wave velocity using a beat-sampling technique. *Ann. Biomed. Eng.*, **16**, 341–347, (1988).
21. Ding, X., Yan, B. P., Karlen, W., Zhang, Y. T., & Tsang, H. K. Pulse transit time based respiratory rate estimation with singular spectrum analysis. *Med. Biol. Eng. Comput.*, **58**, 257–266, (2020).
22. Mukkamala, R. et al. Toward Ubiquitous Blood Pressure Monitoring via Pulse Transit Time: Theory and Practice. *IEEE Trans. Biomed. Eng.*, **62**, 1879-1901, (2015).

23. Kebe, M. et al. Human Vital Signs Detection Methods and Potential Using Radars: A Review. *Sensors*, **20**, 1454, (2020).
24. Q. Lv et al. Doppler Vital Signs Detection in the Presence of Large-Scale Random Body Movements. *IEEE Trans. Microw. Theory Techn.*, **66**, 4261-4270, (2018).
25. Droitcour, A., Lubecke V.,Lin, J. & Boric-Lubecke, O. A microwave radio for Doppler radar sensing of vital signs. *2001 IEEE MTT-S Int. Microw. Symp. Dig.*, **1**, 175-178, (2001).
26. Lubecke, O. B., Ong, P. W. & Lubecke, V. M. 10 GHz Doppler radar sensing of respiration and heart movement. *Proc. IEEE 28th Annu. Northeast Bioeng. Conf*, 55-56, (2002).
27. Wang, J. et al. Noncontact Distance and Amplitude-Independent Vibration Measurement Based on an Extended DACM Algorithm. *IEEE Trans. Instrum. Meas.*, **63**,145-153, (2014).
28. Hu, W., Zhao, Z., Wang, Y., Zhang, H. & Lin, F. Noncontact accurate measurement of cardiopulmonary activity using a compact quadrature Doppler radar sensor. *IEEE Trans. Biomed. Eng.*,**61**, 725-735, (2014).
29. Tu, J. & Lin, J. Fast acquisition of heart rate in noncontact vital sign radar measurement using time-window-variation technique. *IEEE Trans. Instrum. Meas.*, **65**, 112-122, (2016).
30. Sakamoto, T. & Koda, T. Respiratory Motion Imaging Using 2.4-GHz Nine-Element-Array Continuous-Wave Radar. *IEEE Microw. Wireless Compon. Lett.*, **30**, 717-720, (2020).
31. Van, N.T.P., Tang, L., Hasan, S.F., Mukhopadhyay, S., & Minh N.D. Combination of Artificial Intelligence and Continuous Wave Radar Sensor in Diagnosing Breathing Disorder. In: Solanki V., Hoang M., Lu Z., Pattnaik P. (eds) *Intelligent Computing in Engineering. Advances in Intelligent Systems and Computing*, **1125**, Springer, Singapore, 853-863, (2020).
32. Seflek, I., Acar, Y. E., & Yaldiz, E. Small Motion Detection and Non-Contact Vital Signs Monitoring with Continuous Wave Doppler Radars. *Elektronika Ir Elektrotechnika* **26**, 54-60, (2020).
33. Sekak, F. *et al.* Cyclostationary-Based Vital Signs Detection Using Microwave Radar at 2.5 GHz. *Sensors* **20,** 3396 (2020).
34. Malešević, N. *et al.* Contactless Real-Time Heartbeat Detection via 24 GHz Continuous-Wave Doppler Radar Using Artificial Neural Networks. *Sensors* **20,** 2351 (2020)
35. Schires, E., Georgiou, P. & Lande, T. S. Vital sign monitoring through the back using an UWB impulse radar with body coupled antennas. *IEEE Trans. Biomed. Circuits Syst.***12**, 292-302, (2018).
36. Lee, Y. *et al.* A Novel Non-contact Heart Rate Monitor Using Impulse-Radio Ultra-Wideband (IR-UWB) Radar Technology. *Sci Rep* **8,** 13053 (2018).
37. Wang, G., Muñoz-Ferreras, J.-M., Gu, C., Li, C. & Gómez-García, R. Application of linear-frequency-modulated continuous-wave (LFMCW) radars for tracking of vital signs. *IEEE Trans. Microw. Theory Techn.*, **62** 1387-1399, (2014).
38. Wang, S. *et al*. A novel ultra-wideband 80 GHz FMCW radar system for contactless monitoring of vital signs. *Proc. IEEE 37th Annu. Int. Conf. Eng. Med. Biol. Soc.,* 4978-4981, (2015).
39. He, M., Nian, Y. & Gong Y. Novel signal processing method for vital sign monitoring using FMCW radar. *Biomed. Signal Process. Control*, **33**, 335-345, (2017).
40. Ahmad, A., Roh, J. C., Wang, D. & Dubey, A. Vital signs monitoring of multiple people using a FMCW millimeter-wave sensor. *2018 IEEE Radar Conf.*, 1450-1455, (2018).
41. Ebrahim, M. P. *et al*. Systolic Blood Pressure Estimation Using Wearable Radar and Photoplethysmogram Signals. *2019 IEEE Int. Conf. Syst. Man Cybern.*, 3878-3882, (2019).
42. Pour Ebrahim, M. *et al.* Blood Pressure Estimation Using On-body Continuous Wave Radar and Photoplethysmogram in Various Posture and Exercise Conditions. *Sci Rep* **9,** 16346 (2019).
43. Heydari, Fatemeh, et al. "Clinical study of a chest‐based cuffless blood pressure monitoring system." *Med Devices Sens*. **3**, e10091, (2020).

44. Ohata, T., Ishibashi, K., & Sun, G. Non-Contact Blood Pressure Measurement Scheme Using Doppler Radar. *2019 41st Annu. Int. Conf. IEEE Eng. Med. Biol. Soc.*, 778–781, (2019).
45. Stergiou, G. S., *et al.* A Universal Standard for the Validation of Blood Pressure Measuring Devices: Association for the Advancement of Medical Instrumentation/European Society of Hypertension/International Organization for Standardization (AAMI/ESH/ISO) Collaboration Statement. *Hypertens.*,**71**,368-374. (2018).
46. Chavan, M. S., Agarwala, R. A. & Uplane, M. D. Design and implementation of digital FIR equiripple notch filter on ECG signal for removal of power line interference. *WSEAS Trans. Sig. Proc.* **4**, 221–230, (2008).
47. Romanca M. & Szabo, W. Electrocardiogram Pre-Processing, For The Removal Of High Frequency And Power Line Frequency Noise. *Proc. 6th Int. Conf. Optimization of Electrical and Electronic Equipments*, 703-706, (1998).
48. Dotsinsky, I., & Christov, I. Power-line interference subtraction from the electrocardiogram in the presence of electromyogram artifacts. *Electrotechniques & Electronics E+ E*, **1**, 18-21, (2002).
49. Lenis, G., Pilia, N., Loewe, A., Schulze, W. H., & Dössel, O. Comparison of Baseline Wander Removal Techniques considering the Preservation of ST Changes in the Ischemic ECG: A Simulation Study. *Comput. Math. Methods Med., 2017*, 9295029, (2017).
50. Bagha, S. & Shaw, L. A real time analysis of PPG signal for measurement of SpO2 and pulse rate. *Int. J. Comput. Appl.*, **36**, 45–50, (2011).
51. Ram, M. R., Madhav, K. V., Krishna, E. H., Reddy, K. N & Reddy, K. A. On the performance of Time Varying Step-size Least Mean Squares(TVS-LMS) adaptive filter for MA reduction from PPG signals. *2011 Int. Conf. Commun. Signal Process.*, 431-435, (2011).
52. Lee, C. M. & Zhang, Y. T. Reduction of motion artifacts from photoplethysmographic recordings using a wavelet denoising approach. *Proc. IEEE EMBS Asian-Pacific Conf. Biomed. Eng.*, 194 - 195, (2003).
53. Kim, B. S. & Yoo, S. K. Motion artifact reduction in photoplethysmography using independent component analysis. *IEEE Trans. Biomed. Eng.*, **53,** 566-568, (2006).
54. Reddy K. A., George B. & Kumar V. J. Use of Fourier Series Analysis for Motion Artifact Reduction and Data Compression of Photoplethysmographic Signals. *IEEE Trans. Instrum. Meas.*, **58**, 1706-1711, (2009).
55. Reddy, K. A. Novel methods for performance enhancement of pulse oximeters. *PhD thesis*, Indian Institute of Technology, Madras, India.
56. A. Esmaili, M. Kachuee, M. Shabany, Nonlinear Cuffless Blood Pressure Estimation of Healthy Subjects Using Pulse Transit Time and Arrival Time, IEEE Transactions on Instrumentation and Measurement, 2017.

Acknowledgements

This study is supported under the RIE2020 Industry Alignment Fund – Industry Collaboration Projects (IAF-ICP) Funding Initiative, as well as cash and in-kind contribution from Singapore Telecommunications Limited (*Singtel*), through Singtel Cognitive and Artificial Intelligence Lab for Enterprises (SCALE@NTU).

Author contributions

SRI and MFK jointly conceived the idea. SRI, LZ and MPM designed the system and built the experimental setup. SRI and MPM performed the experiments. SRI, MFK, AA, LAQ and MYS assisted with the theory.

All authors contributed to the discussion of experimental results. LZ, AA, MYS, LAQ. and MFK supervised and coordinated all the work. SRI and MFK wrote the manuscript with contributions from all co-authors